



	<b>Experiment title:</b> Temperature dependent Fe 1s2p RIXS-LD on Fe <sub>3</sub> O <sub>4</sub> thin film	<b>Experiment number:</b> HC-2266
<b>Beamline:</b> ID26	<b>Date of experiment:</b> from: 3/02/2016 to: 9/02/2016	<b>Date of report:</b>
<b>Shifts:</b>	<b>Local contact(s):</b> Sara Lafuerza	<i>Received at ESRF:</i>
<b>Names and affiliations of applicants (* indicates experimentalists):</b> Ad van der Eerden [1] Ahmed Ismail [1] Hebatalla Elnaggar [1] Marte van der Linden [1] Patric Zimmermann [1] [1] Debye Institute for Nanomaterials Science, Utrecht University		

**Outline:**

1. Objectives
2. Experiment details
  - 2.1 Samples
  - 2.2 Beamline configuration
  - 2.3 Setups
3. Preliminary results
  - 3.1 Room temperature measurement
  - 3.2 High temperature measurement
4. Conclusion
5. Future work
6. References

## 1. Objectives

The goal of this experiment is to measure angular dependent Fe 1s2p Resonant Inelastic X-ray Scattering (RIXS) on single crystal  $\text{Fe}_3\text{O}_4$  below and above the Curie temperature ( $T_C \sim 858\text{K}$ ). We aim to address the following points through our measurement:

1. Assign spectral features to specific Fe sites taking advantage of the spectral details revealed in the RIXS-LD planes on the basis of ligand field multiplet calculations.
2. Map the symmetry of the unoccupied orbitals from the measurement of the  $360^\circ$  angular behaviour of the dichroic features. The orbital selectivity of the angular dependence combined with the site selectivity of Fe 1s2p RIXS enables us to probe site selectively the symmetry of the unoccupied orbitals.
3. Disentangle the interplay between structural and magnetic dichroism by following the temperature dependence of the dichroic signal below and above the  $T_C$  of  $\text{Fe}_3\text{O}_4$ .
4. Validate the theoretical angular dependence of the RIXS cross-section in the presence and absence of exchange field.

## 2. Experiment details

### 2.1 Samples

Magnetite is a naturally occurring metastable form of iron oxide that has a chemical formula of  $\text{Fe}_3\text{O}_4$ . It crystallizes in a cubic (isometric) crystal system, with the oxide anions arranged in a cubic close-packed lattice. The cations ( $\text{Fe}^{2+}$  and  $\text{Fe}^{3+}$ ) are arranged in an inverse spinel structure such that half of the  $\text{Fe}^{3+}$  cations occupy the octahedral ( $\text{O}_h$ ) sites and the other half occupies the tetrahedral ( $\text{T}_d$ ) sites in the lattice (shown in Figure 1). On the other hand, all the  $\text{Fe}^{2+}$  cations occupy the  $\text{O}_h$  sites. The crystal lattice constant is of  $8.397\text{\AA}$  at standard room conditions.  $\text{Fe}_3\text{O}_4$  is a ferrimagnetic material where the magnetic moments of Fe cations in  $\text{T}_d$  and  $\text{O}_h$  sites are coupled antiferromagnetically.

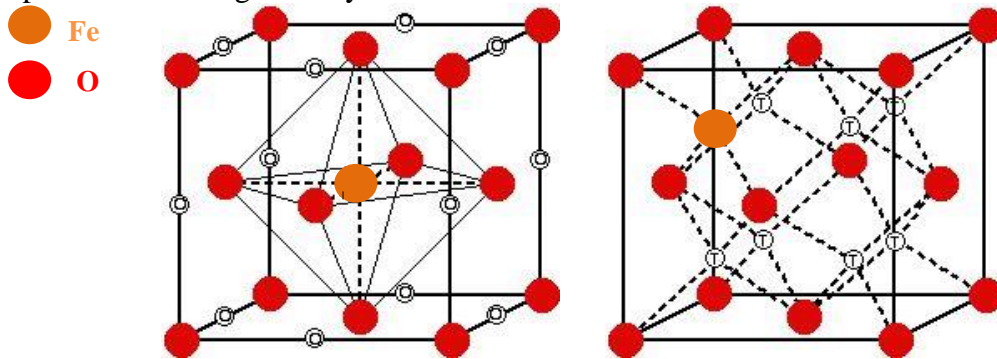


Figure 1: Octahedral sites (left) and tetrahedral sites (right) in a closed pack cubic structure.

The following samples were measured during the beamtime:

Number	Sample	Description
1	$\text{Fe}_3\text{O}_4$ powder	$d < 5\mu\text{m}$ , 95% (from Sigma-Adricht , Product 310069)
2	$\text{Fe}_3\text{O}_4$ (110) natural	Cut and polished to a (110) surface (from SurfaceNet)
3	$\text{Fe}_3\text{O}_4$ (111)	Cut and polished to a (111) surface

	natural	(from SurfaceNet)
4	Fe <sub>3</sub> O <sub>4</sub> (110) synthetic	Cut and polished to a (110) surface (from Instituto de Nanociencia de Aragón)
5	Fe <sub>3</sub> O <sub>4</sub> (111) synthetic	Cut and polished to a (111) surface (from Instituto de Nanociencia de Aragón)
6	Fe <sub>3</sub> O <sub>4</sub> (110) synthetic	Cut and unpolished to a (110) surface (from AGH University of Science and Technology)
7	Fe <sub>3</sub> O <sub>4</sub> (111) synthetic	Cut and unpolished to a (111) surface (from AGH University of Science and Technology)
8	Fe <sub>2</sub> O <sub>3</sub> (001) natural	Cut and polished to (001) surface (from Surface Prep. Lab)

Table 1: Description of samples used during the experiment HC-2266.

## 2.2 Beamline configuration

- The incident energy was selected using a pair of Si(311) crystals for high energy resolution. The spot size on the sample position was 100\*600  $\mu\text{m}^2$ .
- Linear horizontal polarized X-rays were used during the experiment.
- A set of four spherically bent Ge(440) analyzer crystals with masks were used for high resolution ( $\sim 0.5$  eV as deduced from the FWHM of the elastic peaks).
- The spectrometer was set in a back scattering configuration with an angle of 15 degrees from the incident beam in order to maximize the signal seen by the crystals

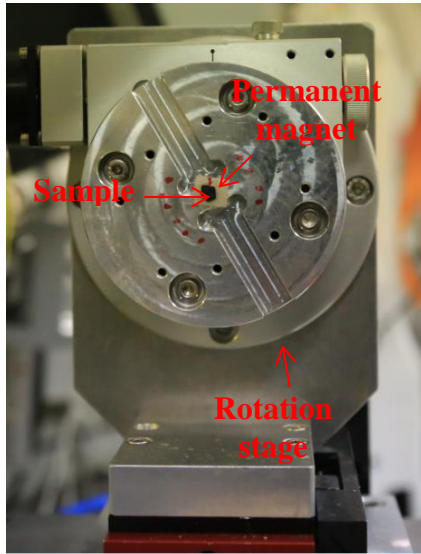
## 2.3 Setups

### 2.3.1 Room temperature setup

The room temperature setup consists of:

- Huber 360 degrees rotational stage.
- Set of permanent magnets.
- Adaptive plate with two possible configurations for mounting the magnets; longitudinal configuration where the magnetic field is parallel to the incident wave vector ( $k$ ) and transverse configuration where the magnetic field is perpendicular to  $k$  (refer to Figure 2).

a) Longitudinal magnetic field



b) Transverse magnetic field

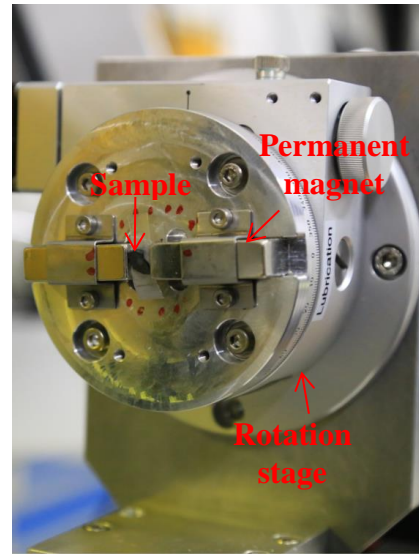


Figure 2: Room temperature setup, *a)* Longitudinal configuration and *b)* Transverse configuration.

### 2.3.2 High temperature setup

The high temperature setup was designed to operate either under vacuum ( $\sim 10^{-6}$  mbar) or under static over-pressure of inert gas (pressure < 1.3 bar inside the furnace) to prevent oxidation of  $\text{Fe}_3\text{O}_4$  at high temperatures. The high temperature setup consists of:

- Huber 360 degrees rotational stage.
- Furnace that can heat up to  $1000^\circ\text{C}$  under vacuum (micro- tomo furnace borrowed from the sample environment).
- Be dome cover (500  $\mu\text{m}$  thick) for the furnace to withstand the temperature and pressure requirements while having satisfactory transmission in the energy range from 6.4 to 7.2 KeV (the dome was borrowed from ID28).
- Slip ring to input the cooling water and the gases to the furnace without having to allow for rotating the furnace without rotating the cooling and gas tubing (DSTI LT-2141).
- Cold  $\text{N}_2$  gun for cooling the Be dome and removing any formed ozone from the surface of the Be dome.
- Vacuum turbo-pump (reaches  $\sim 10^{-7}$  mbar).
- High purity He gas (BIP He,  $\text{O}_2 < 10\text{ppm}$ ) for experiments done under static over-pressure of inert gas.
- Pressure relief valve and a burst disk to regulate the pressure of the inert gas during heating.
- A relay controlled system that switches the heating off if the temperature of the Be window exceeds  $200^\circ\text{C}$ .

The setup design (see Figure 3) allows us to:

- Rotate the sample  $300^\circ$  about the surface normal at high temperatures (upto  $1000^\circ\text{C}$ ) under vacuum ( $\sim 1 \times 10^{-6}$  mbar at  $1000^\circ\text{C}$ ).

- Rotate the sample a full 360° about the surface normal at high temperatures (upto 800°C) working under overpressure inert gas (1.2 bar inside the furnace).

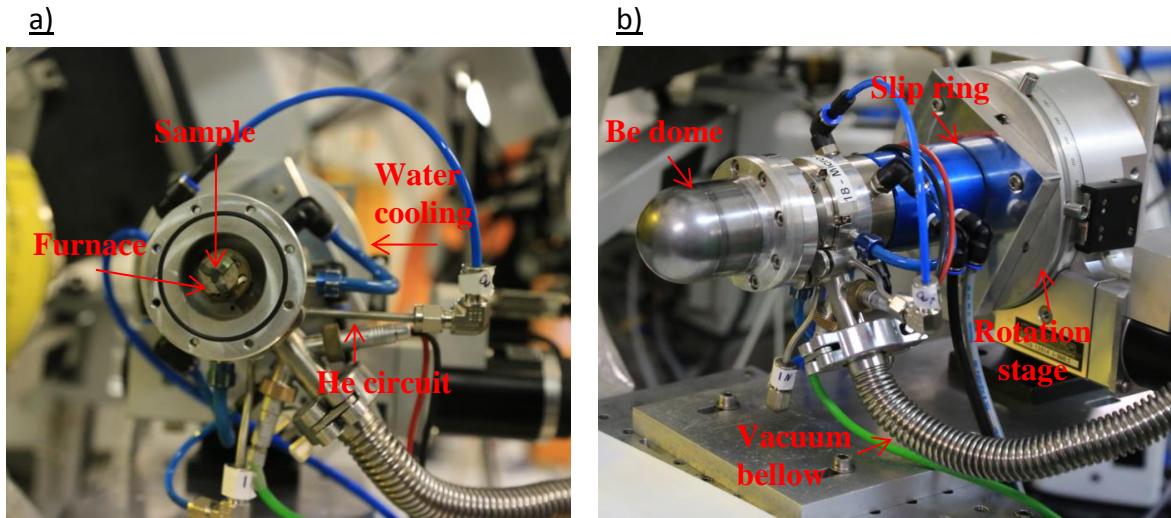


Figure 3: High temperature setup a) without Be dome and b) with the Be dome.

The high temperature setup proved to work well during the first measurements (sample 1 and 2 were successfully measured without oxidation). However, at the end of the experiment, the slip ring malfunctioned and the water cooling circuit leaked water into the He gas circuit. This led to the oxidation of sample 6 at high temperature. In order to avoid such leakages in future experiments, the slip ring will only be used for the water cooling circuit and the gases will be delivered directly to the furnace without using the slip ring.

### 3. Preliminary results

Follows is a list of the performed measurements on the samples:

No.	Room temp. HERFD, XES, EXAFS	Room temp. linear dichroism	Room temp. linear magnetic dichroism	Room temp. RIXS map	High temp. HERFD, XES, EXAFS	High temp. linear dichroism	High temp. RIXS map
1	✓				✓		
2	✓	✓			✓	✓	✓
3	✓	✓					
4	✓	✓	✓	✓			
5	✓	✓	✓	✓			
6	✓	✓	✓	✓	✓	✓	
7	✓	✓	✓	✓			
8	✓	✓	✓	✓	✓	✓	✓

Where HERFD is Fe K edge High energy resolved fluorescence detected X-ray absorption near edge structure measured detecting the  $K_{\alpha 1}$  fluorescence, XES is the Fe  $K_{\alpha 1}$  and  $K_{\alpha 2}$  X-ray emission spectroscopy and EXAFS is the extended X-ray absorption

fine structure measured detecting the  $K_{\alpha 1}$  fluorescence.  $1s2p$  RIXS measurements were done only in the Fe  $K_{\alpha 1}$  region (as the Fe  $K_{\alpha 2}$  is considerably weaker).

### 3.1 Room temperature measurement

#### 3.1.1 (110) $Fe_3O_4$ single crystal in the longitudinal configuration

We show here the results of the (110)  $Fe_3O_4$  sample (sample 6) in the longitudinal magnetic field configuration. In this configuration the magnetic field ( $B$ ) was parallel to the  $[110]$  crystallographic axis. The incident wave vector ( $k_{in}$ ) was parallel to the  $[110]$  crystallographic axis of the sample. The scattered wave vector ( $k_{out}$ ) was along the  $[1\sqrt{3}0]$  crystallographic axis of the sample. The sample was rotated about the  $[110]$  axis for the dichroic measurements (see Figure 4).

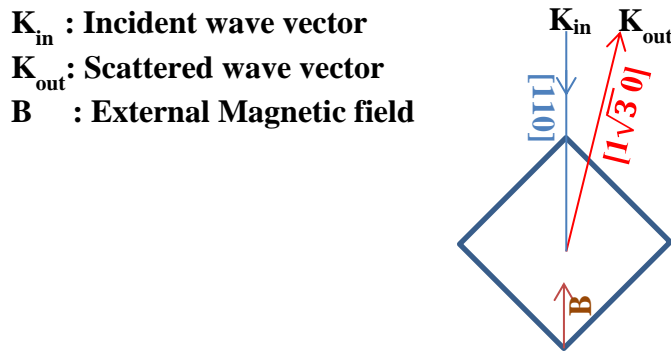


Figure 4: Schematic of the scattering geometry in the crystal coordinates with longitudinal magnetic field for sample 6 (top view).

The linear dichroism is, we measure the signal at two orientations; at angle  $0^\circ$  (shown in Figure 4) and rotating  $90^\circ$  about the  $[110]$  axis. Figure 5a) (and b) shows HERFD XANES (XES) for the two orientations and the dichroism signal. Three dichroic features can be seen in the pre-edge region (7.110-7.117 KeV) and only the Fe  $K_{\alpha 1}$  shows visible dichroism with the current statistics.

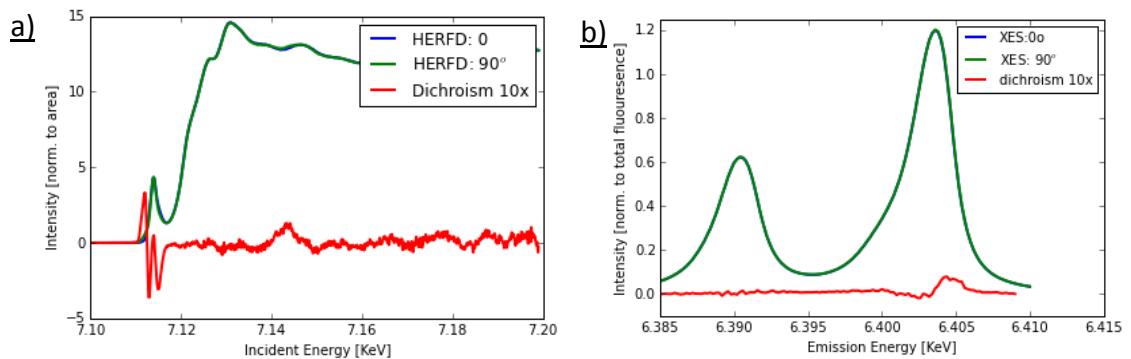


Figure 5: a) Fe  $1s2p$  HERFD XANES and b)  $K_{\alpha}$  XES of (110)  $Fe_3O_4$  single crystal in the longitudinal magnetic field configuration.

In order to understand the dichroic feature in more detail, we measure angular dependent  $1s2p$  RIXS for the same configurations (Figure 6). Figure 7 shows four main RIXS magnetic linear dichroism (MLD) features in the pre-edge region. Rotating the sample a full  $360^\circ$  shows a pure quadrupole angular behaviour for all features except that at incident energy = 7.1141 KeV and emission energy of 6.4044 KeV (shown in green in Figure 7b).

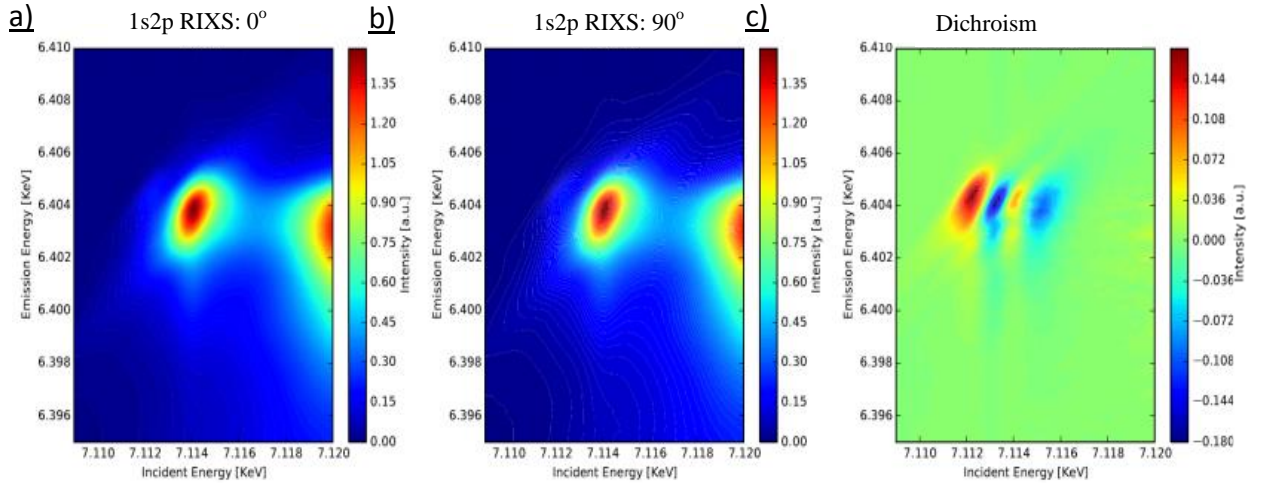


Figure 6: *Fe 1s2p RIXS of (110) Fe<sub>3</sub>O<sub>4</sub> single crystal in the longitudinal magnetic field configuration: a) at 0°, b) at 90° and c) the dichroism signal.*

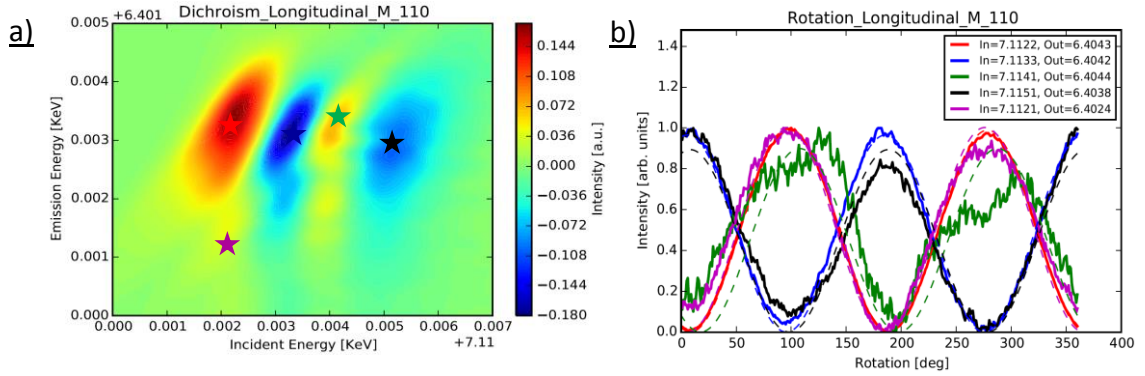


Figure 7: *a) A zoom of the Fe 1s2p RIXS MLD pre-edge signal. b) Full rotation scans about the [110] axis at the centre of the dichroic features (i.e. at constant incident and emission energies). The energy positions of the rotational scans are also shown in coloured stars on the dichroism map.*

We assign the three features at incident energies: 7.1122, 7.1133 and 7.1151 KeV to Fe<sup>2+</sup> O<sub>h</sub> sites based on crystal field multiplet (CFM) calculations of K pre-edge absorption (XAS). Figure 8a and b show the calculated angular dependence of the three pre-edge features about the [110] crystallographic axis. The angular behaviour could be visualised by plotting the overlap between the single electrons d-orbitals and the incident light. The t<sub>2g</sub> and e<sub>g</sub> orbitals show a C<sub>2</sub> symmetry about k (see Figure 8c and d). It can be seen that the t<sub>2g</sub> and e<sub>g</sub> orbitals probed by the incident light are 90° phase shifted.

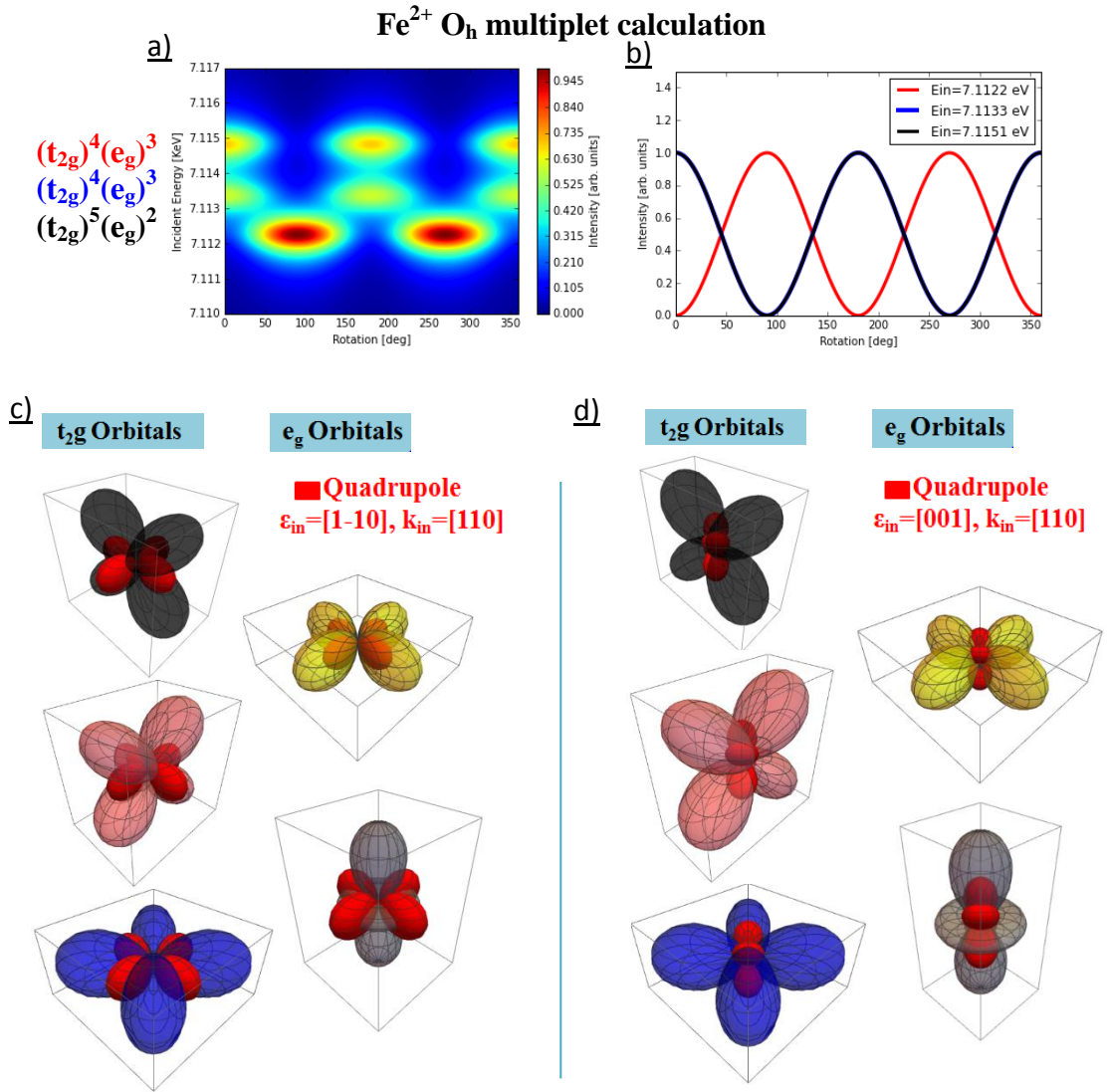


Figure 8: a): Crystal field multiplet calculation for the Fe<sup>2+</sup> O<sub>h</sub> sites in Fe<sub>3</sub>O<sub>4</sub> ( $10Dq=1.2$ eV,  $M=0.01$ eV, SOC=100%). a): The angular dependence XAS rotating the sample about the [110] crystallographic axis. b): Horizontal cuts showing the angular behaviour of the three features. c): Spherical harmonics showing the overlap between the single-electron  $d$  orbitals in cubic crystal field and the quadrupole light with  $k_{in}//[110]$  and  $\epsilon_{in}//[1-10]$  crystallographic axes. d): Spherical harmonics showing the overlap between the single-electron  $d$  orbitals in cubic crystal field and the quadrupole light with  $k_{in}//[110]$  and  $\epsilon_{in}//[001]$  crystallographic axes.

### 3.1.2 (110) Fe<sub>3</sub>O<sub>4</sub> single crystal in the transverse configuration

We present here the results of the (110) Fe<sub>3</sub>O<sub>4</sub> sample (sample 6) in the transverse magnetic field configuration. In this configuration the magnetic field (B) was parallel to the [0.54 -0.54 0.64] crystallographic axis. The incident wave vector ( $k_{in}$ ) was parallel to the [110] crystallographic axis of the sample. The scattered wave vector ( $k_{out}$ ) was along the  $[1\sqrt{3}0]$  crystallographic axis of the sample. The sample was rotated about the [110] axis for the dichroic measurements. The angular dependent 1s2p RIXS for the same configurations is shown in Figure 9. Figure 10 shows four main RIXS MLD features in the pre-edge region. Rotating the sample a full 360° shows a pure

quadrupole angular behaviour for all features except that at incident energy = 7.1143 KeV and emission energy of 6.40537 KeV (shown in black in Figure 10b).

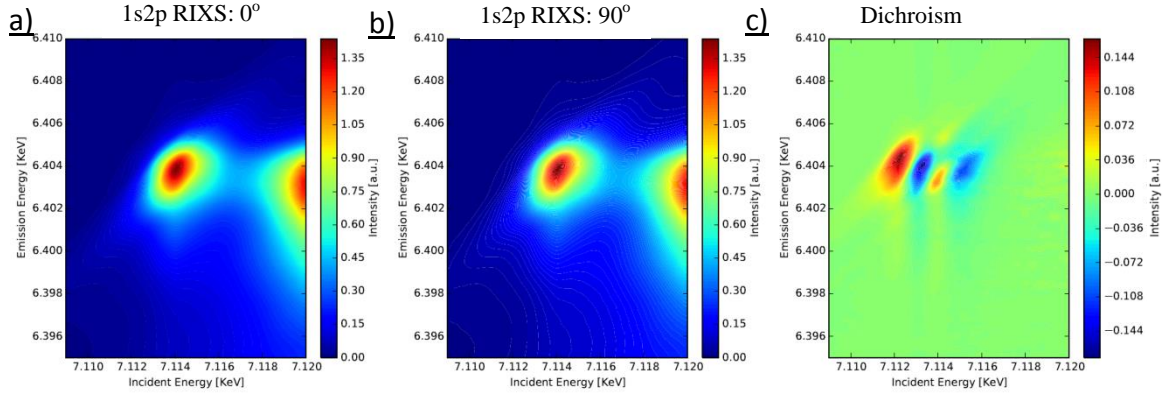


Figure 9: *Fe 1s2p RIXS of (110) Fe<sub>3</sub>O<sub>4</sub> single crystal in the transverse magnetic field configuration: a) at 0°, b) at 90° and c) the dichroism signal.*

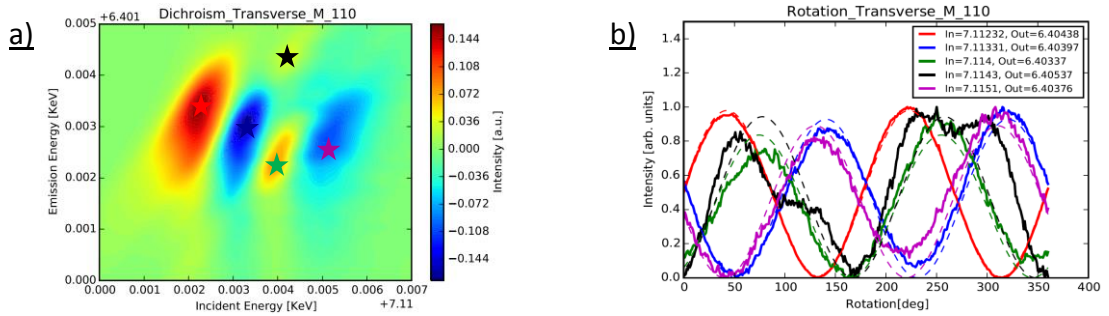


Figure 10: *a) A zoom of the Fe 1s2p RIXS MLD pre-edge signal. b) Full rotation scans about the [110] axis at the centre of the dichroic features (i.e. at constant incident and emission energies). The energy positions of the rotational scans are also shown in coloured stars on the dichroism map.*

It can be seen that the features at incidence energy 7.11331 and 7.1151 KeV are not overlapping as in Figure 7b. Comparing with this result with CFM calculations of the three Fe sites in Fe<sub>3</sub>O<sub>4</sub> (Figure 11), we observe this shift for the Fe<sup>2+</sup> O<sub>h</sub> sites with spin-orbit coupling of the 3d valence electrons=100%. Thus we conclude that the shift is a sensitive probe of the spin-orbit coupling and the exchange field interaction.

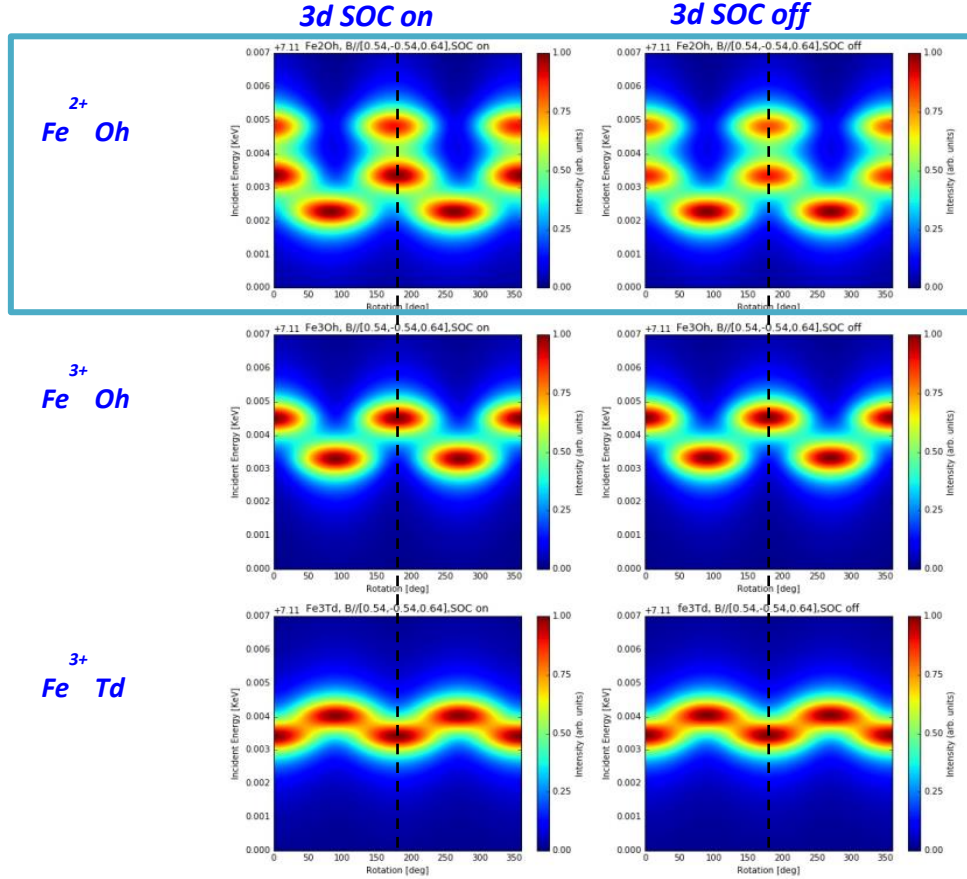


Figure 11: Crystal field multiplet calculation for the  $Fe^{2+} O_h$  sites ( $10Dq=1.2eV$ ,  $M=0.01eV$ ),  $Fe^{3+} O_h$  sites ( $10Dq=1.2eV$ ,  $M=0.01eV$ ) and  $Fe^{3+} T_d$  sites ( $10Dq=-0.6eV$ ,  $M=0.01eV$ ) in  $Fe_3O_4$ : a) with spin-orbit coupling of the 3d valence electrons=100% and b) with spin-orbit coupling of the 3d valence electrons=0%.

## 3.2 High temperature measurement

In an attempt to gain a better understanding of the linear dichroism signal, we study RIXS-LD as a function of temperature. The long range order of the magnetic moments of Fe in  $Fe_3O_4$  is destroyed at temperatures higher than the Curie temperature ( $T_C \sim 858K$ ). Making use of the fact that the crystal field dichroism should not exhibit any temperature dependence, in contrast with the magnetic part which scales with  $\langle M^2 \rangle$ , helps us disentangle both effects and determine their relative strength.

### 3.2.1 (110) $Fe_3O_4$ powder

Figure 12 shows the HERFD XANES scans as a function of temperature during heating scans. The sample was heated up to  $988^\circ C$  in vacuum ( $\sim 10^{-6}$  mbar). Some spectral changes could be seen in the pre-edge region. Comparing the spectral shape of the  $Fe_3O_4$  at  $988^\circ C$  to  $Fe_2O_3$ , we conclude that the sample did not oxidise (Figure 13). This could also be confirmed from the phase diagram shown in Figure 14. This measurement confirmed that the setup works however no angular dependences could be measured for this sample because it is a powder.

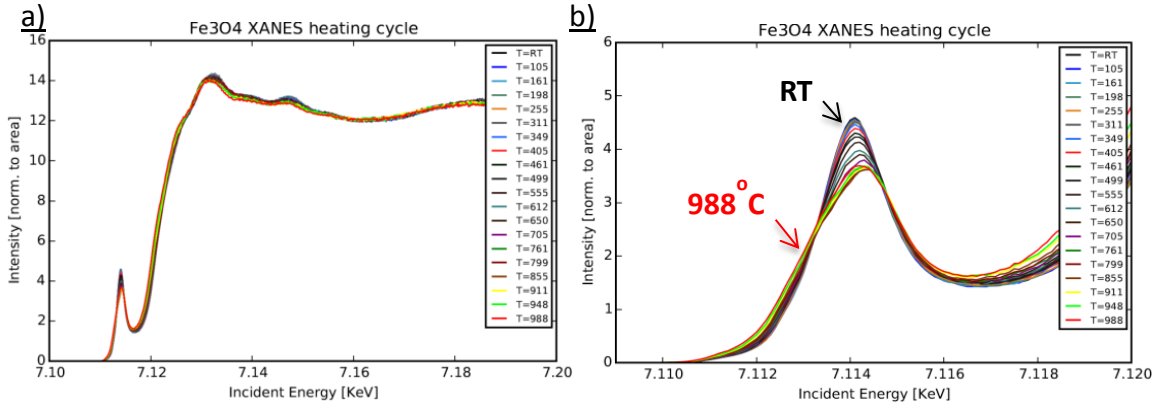


Figure 12: a) HERFD XANES of Fe K edge of  $Fe_3O_4$  powder as a function of temperature. b) A zoom at the pre-edge.

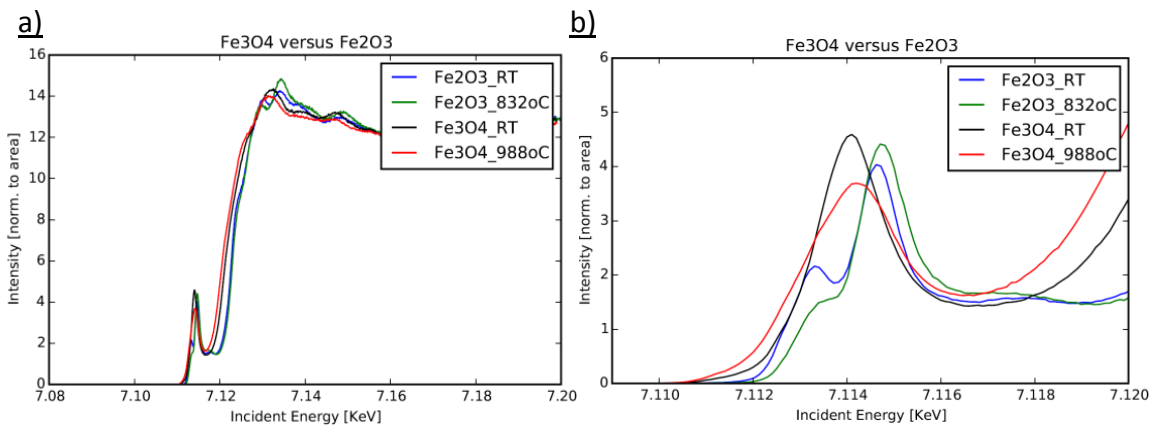


Figure 13: a) HERFD XANES of Fe K edge of  $Fe_3O_4$  and  $Fe_2O_3$  powder at room and high temperature. b) A zoom at the pre-edge.

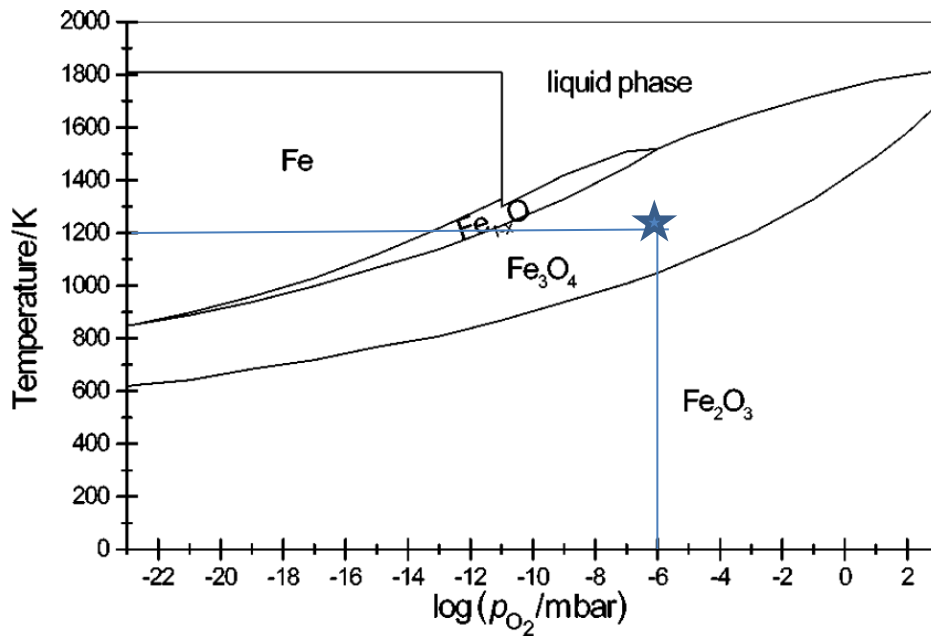


Figure 14: Phase diagram (temperature-pressure) of Fe. The final conditions shown in blue suggests that Fe should be in the  $Fe_3O_4$  phase.

### 3.2.2 (110) Fe<sub>3</sub>O<sub>4</sub> natural crystal

Figure 15 shows the HERFD XANES scans as a function of temperature during heating scans of sample 2. The sample was heated up to 898°C in vacuum ( $\sim 10^{-6}$  mbar). The same spectral changes could be seen in the pre-edge region. However, the quality of the natural commercial crystal is not good (possibly the crystal has many defects and high mosaicity) as no angular dependence could be observed at room temperature or high temperature (Figure 16).

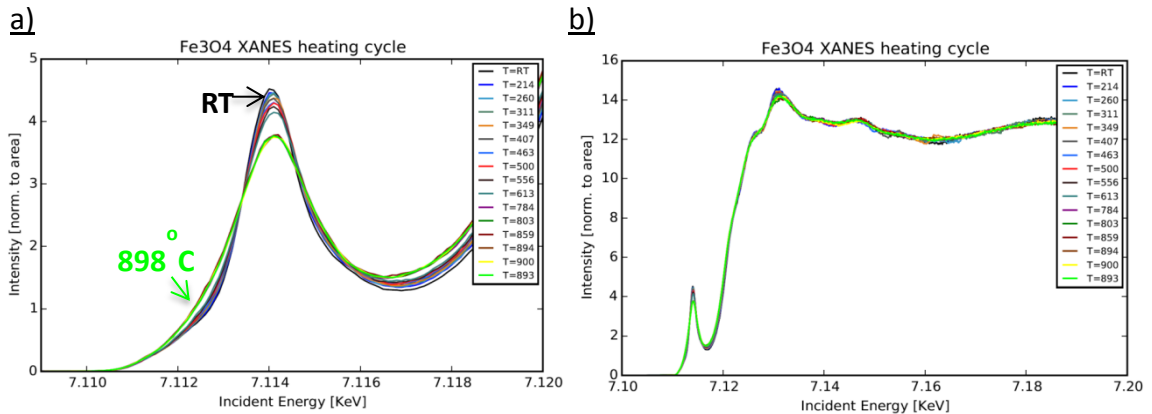


Figure 15: a) HERFD XANES of Fe K edge of Fe<sub>3</sub>O<sub>4</sub> natural single crystal at room and high temperature. b) A zoom at the pre-edge.

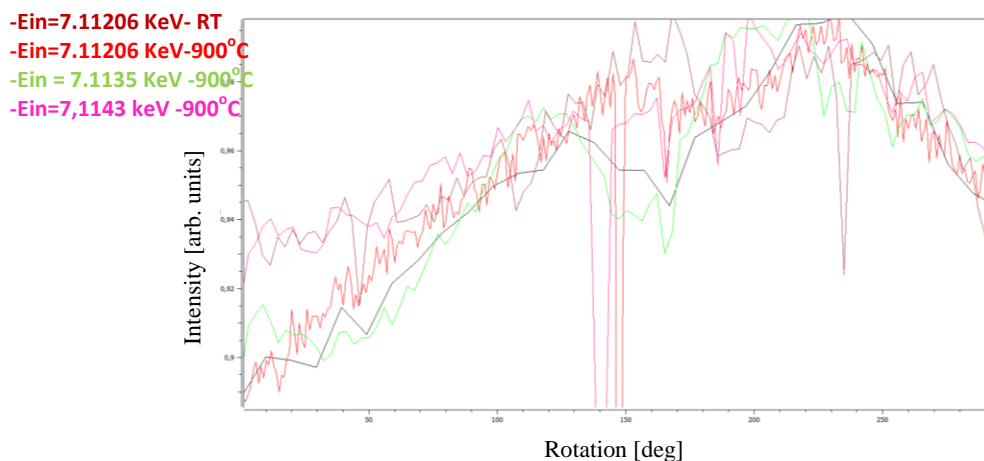


Figure 16: Angular behaviour of the pre-edge features of Fe<sub>3</sub>O<sub>4</sub> natural crystal.

### 3.2.3 (110) Fe<sub>3</sub>O<sub>4</sub> single crystal

Figure 17 shows the pre-edge region of HERFD XANES of (110) Fe<sub>3</sub>O<sub>4</sub> single crystal (sample 6). As can be seen, the sample is oxidized at 900°C and the pre-edge looks like that of Fe<sub>2</sub>O<sub>3</sub> (shown in brown). This is because the slip ring leaked water vapour into the furnace.

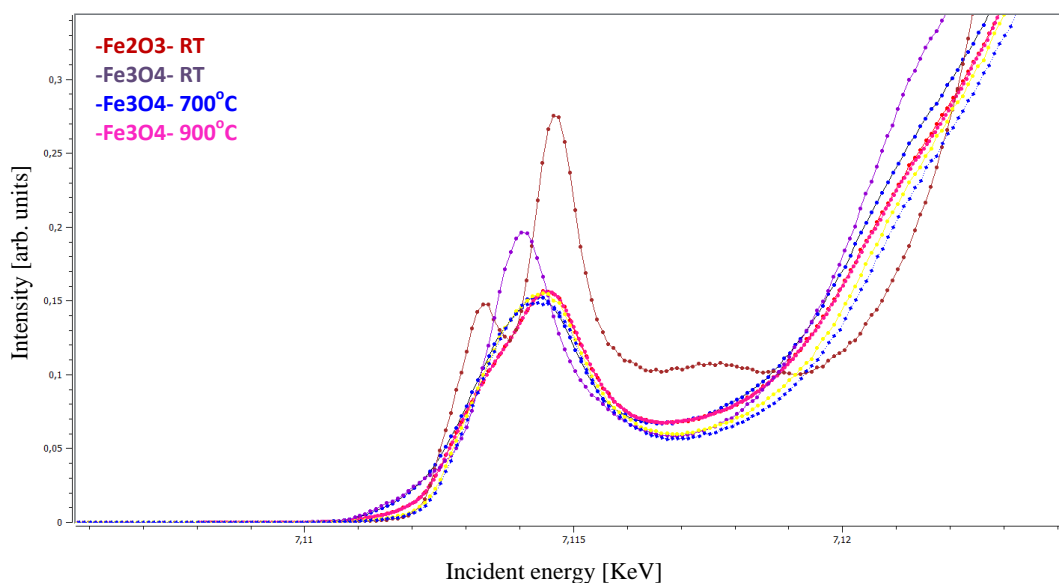


Figure 17: HERFD XANES of Fe K edge of  $\text{Fe}_3\text{O}_4$  single crystal at room and high temperature. The pre-edge of  $\text{Fe}_2\text{O}_3$  single crystal is shown in brown for comparison.

## 4. Conclusions

- Using 1s2p RIXS linear dichroism, we are able to reveal the  $1s \rightarrow 3d$  quadrupole pre-edge transitions that are otherwise suppressed by the dipole allowed transition at the  $\text{Fe}^{3+} \text{T}_d$  sites of  $\text{Fe}_3\text{O}_4$ .
- Using the orbital selectivity of angular dependent RIXS, we map the unoccupied valence orbitals of selective sites (**Error! Reference source not found.** focusing on the three pre-edge features which we assign to  $\text{Fe}^{2+}$  sites of  $\text{Fe}_3\text{O}_4$  based on multiplet calculations).
- Using 1s2p RIXS magnetic dichroism, we can sensitively probe the spin-orbit and exchange field interactions at the  $\text{Fe}^{2+}$  sites of  $\text{Fe}_3\text{O}_4$ .

## 5. Future work

The high temperature experiment has been attempted in HC-2266 and proofed initially to work, however due to a malfunction of an equipment (slip ring provided by the ESRF),  $\text{Fe}_3\text{O}_4$  oxidized to  $\alpha\text{-Fe}_2\text{O}_3$  at high temperatures and therefore we would like to reinvestigate this part. In addition, we plan to investigate Co and Zn doped  $\text{Fe}_3\text{O}_4$  single crystals to elucidate the local charge on each Fe site.  $\text{Co}^{2+}$  has a strong affinity to occupy  $\text{O}_h$  sites forming a  $\text{CoFe}_2\text{O}_4$  inverse spinel structure while  $\text{Zn}^{2+}$  occupies  $\text{T}_d$  sites forming  $\text{ZnFe}_2\text{O}_4$  direct spinel. Comparison of the RIXS-LD signal from the different compounds enables us to assign spectral features to specific Fe sites.